Journal of Power Sources 274 (2015) 355–366

Contents lists available at ScienceDirect

Journal of Power Sources

journal homepage: www.elsevier.com/locate/jpowsour

Fuzzy modelling for the state-of-charge estimation of lead-acid batteries

Claudio Burgos, Doris Sáez*, Marcos E. Orchard, Roberto Cárdenas

Department of Electrical Engineering, Faculty of Mathematical and Physical Sciences, University of Chile (DIE), Av. Tupper 2007, 8370451 Santiago, Chile

HIGHLIGHTS

- A novel fuzzy model is proposed to characterise lead-acid battery discharging.
- An extended Kalman filter based on a fuzzy model is proposed for SoC estimation.
- The polarisation resistance can be estimated using this novel algorithm.
- Experimental validation of the proposed methodology is presented and discussed.

ARTICLE INFO

Article history:
Received 6 July 2014
Received in revised form
3 October 2014
Accepted 6 October 2014
Available online 15 October 2014

Keywords:
State-of-charge
Lead-acid batteries
Fuzzy modelling
Extended Kalman filter

ABSTRACT

This paper introduces a novel fuzzy model based structure for the characterisation of discharge processes in lead-acid batteries. This structure is based on a fuzzy model that characterises the relationship between the battery open-circuit voltage (Voc), the state of charge (SoC), and the discharge current. The model is identified and validated using experimental data that is obtained from an experimental system designed to test battery banks with several charge/discharge profiles. For model identification purposes, two standard experimental tests are implemented; one of these tests is used to identify the Voc–SoC curve, while the other helps to identify additional parameters of the model. The estimation of SoC is performed using an Extended Kalman Filter (EKF) with a state transition equation that is based on the proposed fuzzy model. Performance of the proposed estimation framework is compared with other parametric approaches that are inspired on electrical equivalents; e.g., Thevenin, Plett, and Copetti.

© 2014 Elsevier B.V. All rights reserved.

1. Introduction

The estimation of the remnant energy stored in Battery Energy Storage Systems (BESS) is important for the evaluation of its future performance. In this regard, many different battery-based applications have considered the problem of State-of-Charge (SoC) estimation; e.g., microgrids [1], electric cars [2], wind-diesel systems, distribution grids [3], and Flexible Alternate Current Transmission Systems (FACTS). Moreover, in microgrids, the SoC is usually an input of the energy management system [1] and it is required to optimise its performance. Additionally, the SoC is also an important parameter for an adequate operation of electric cars and drones, because it provides information that helps to estimate their respective autonomy.

The SoC may be considered as the remnant energy in a battery bank. The SoC is usually defined as a value in the interval [0,1], where 0 indicates complete discharge of the battery and 1, full charge. This work focuses on the problem of estimating the SoC in lead-acid Batteries; a variable that is affected by charge/discharge rates, temperature, usage time, hysteresis and self-discharge effects (due to the internal impedance of the cell). There are a number of aspects that have to be considered when implementing SoC estimation procedures, and in this regard, we will solely focus on: (i) the model of the battery that will be used, and (ii) the algorithm that will be utilised to estimate parameters in non-linear/non-observable systems. Several research efforts aim at providing a solution for these issues using empirical, physicochemical, or electric models in conjunction with estimation techniques based on fuzzy logic [4], neural networks [5], or Bayesian approaches such as the Extended Kalman Filter (EKF) [6,7] and particle filtering [8].

One of the main difficulties for SoC estimation is that the SoC cannot be directly measured in a battery-based storage system. Therefore, this value must be inferred from the observation of other

* Corresponding author.
E-mail address: dsaez@ing.uchile.cl (D. Sáez).

http://dx.doi.org/10.1016/j.jpowsour.2014.10.036
0378-7753/© 2014 Elsevier B.V. All rights reserved.

variables such as the battery current, voltage, temperature, State-of-Health (SoH) [8], and indicators associated with the self-discharge phenomena [9–12]. The utilisation of more complex electrochemical models for the estimation of the SoC is also possible. However these techniques are only suitable for off-line studies, mainly because these models (i) require a large number of variables to represent the battery internal processes, (ii) assume extremely accurate measurements [5,9], and (iii) have an elevated computational cost [5,9]. Other options for SoC monitoring include the open-circuit voltage (Voc) method [13]; where an equivalent circuit model is developed using resistors, capacitors and voltage sources to form a circuit network (such as polarisation-impedance-based models or Thevenin-equivalent-based models). This approach has the advantage of providing a direct relationship between battery SoC and voltage measurements – the higher the Voc, the higher the SoC [14]. Unfortunately, the implementation of this test requires long battery resting periods, and limiting its use for online applications [5,9,12,14]. Similarly, Electrochemical Impedance Spectroscopy (EIS) [9,15] is outlined as a non-invasive method that intends to provide a complete characterisation of the battery internal equivalent circuit. However, the implementation of an EIS test requires the acquisition of costly equipment (usually available only at laboratory test sites), which severely limits its wide spread use in practice [16]. Moreover, data obtained using EIS, usually is very noisy [6,16]. It is for this reason that current research efforts are mostly focused on the development of SoC estimation algorithms based on empirical models that incorporate relevant phenomenological aspects of the process; i.e., the relationship between currents, voltages and temperatures of cells. Among these methods, it is worth mentioning those that are based on fuzzy logic, neural networks, and Bayesian approaches.

Fuzzy logic models have been used for SoC estimation mainly for the identification of battery from EIS data [4,17,18] and to a lesser degree, directly from voltage or discharge current measurements. Salkind et al. in Ref. [4] propose a SoC estimator based on fuzzy models for two battery storage systems: lithium/sulphur dioxide and nickel/metal hydride. In this estimator, the relationships between the imaginary component of the impedance at 10.3 Hz, 41.01 Hz and 4101 Hz and the SoC of the cell are modelled using a Sugeno fuzzy system. A similar approach for the SoC estimation of a Ni/MH battery is presented in Ref. [17]. This paper also considers the relationship between the imaginary component of the impedance and the SoC using fuzzy clustering to obtain of the corresponding fuzzy sets. Zenati et al. in Ref. [18] propose to use EIS measurements for the SoC estimation of Li-Ion batteries. The experimental work discussed in this paper considers temperature variations and several battery charging levels. The influence of DC current over the AC impedance during EIS measurement is analysed and interpreted by a fuzzy system. The methods proposed in Refs. [4,17,18] could be used for on-line estimation of the SoC. However, it requires access to electrochemical impedance spectroscopy (EIS) data. Moreover, because of the EIS disadvantages previously discussed, methods to characterise the SoC using voltage and current measurements have more advantages. In this regard, a different approach that generates a SoC estimator from voltage recovery profiles, without the need of impedance measurements, is presented in Ref. [19]. Particularly, this method uses the minimum battery voltage, at a fixed load current, as one of the fuzzy system inputs. The other input is the difference between the maximum and minimum voltage of the battery pack. This methodology is proposed in Ref. [19] to estimate the SoC in batteries that undergo constant charge/discharge profiles as for instance in batteries used to feed portable defibrillators.

Another fuzzy logic based SoC estimator for lead-acid batteries is presented in Ref. [20]. In this case, an improved Coulomb metric is augmented with a fuzzy inference rule which considers both the temperature and the battery current level. However, the proposed estimator is only validated by simulation experiments and it is not tested with real data from an experimental system.

Neural networks have also been used to represent a non-linear relationship between battery measurements respect to the evolution of SoC in time; however, they usually require huge data sets for the identification process [9,5,11]. A neuro-fuzzy system is proposed for estimation of the SoC of a Li-Ion battery in Ref. [21]. The data is collected using Hybrid Pulse Power Characterisation (HPPC) tests specified in the standard “Partnership for a new Generation of Vehicles” [22]. In Ref. [21] an adaptive neuro-fuzzy inference system (ANFIS) models the relation between SoC and the open circuit voltage. Given that the estimator input corresponds to the Voc, this method is not suitable for on-line application. A slightly different approach was presented in Refs. [23], where ANFIS models and Principal Components Analysis (PCA) are used to estimate the SoC of Ni-MH batteries. In this method, the main inputs of the ANFIS estimator are the discharge current, battery terminal voltage and the battery energy released. According with Ref. [23] the proposed neuro-fuzzy model has several advantages when compared with conventional neural network estimator. However, huge data sets are required for training the large number of parameters required by the proposed ANFIS system. This may produce a substantial increase in the requirements associated with the implementation.

A new learning structure called Merged Fuzzy Neural Network (MFNN) is proposed in Ref. [24] to estimate the SoC of a lithium-ion battery bank. The SoC of each battery cell is modelled by a neural network using the battery terminal voltage, discharge current and battery surface temperature as inputs. The parameters of the MFNN are obtained using genetic algorithms. Although this new approach allows the modelling of the whole battery bank, a very large data set is required because measurements in each cell have to be realised. Therefore, the complexity of this model is high, increasing the difficulties associated with a real time implementation.

In recent years there has been a growing interest in the use of stochastic filtering techniques (unscented Kalman Filter [25], extended Kalman Filter [6,7], and unscented particle filter [26]) to estimate the SoC of battery cells. In fact, experience has demonstrated that Bayesian estimators are well suited for real-time estimation problems that incorporate dynamic state transition models [6,8,16]. Particularly related to the proposed problem is a Stochastic Fuzzy Neural Network (SFNN) presented in Ref. [27] to model the Ni-MH battery behaviour. The SoC is estimated with extended Kalman filters based on SFNN models. The load voltage is modelled by the SFNN considering the charge and discharge currents, temperature and SoC as inputs. The SFNN has a filtering effect on the inputs and this improves the signal to noise relationship of the output signals. In this case the validation discharge profile is very similar to the training set. Therefore, the methodology proposed in Ref. [27] has not been fully validated for different battery operating conditions.

Particularly in this work, a novel estimator of the SoC for a lead-acid battery bank is proposed. The SoC estimator is based on an Extended Kalman Filter (EKF) that uses a fuzzy model as its observation equation. The scheme of the proposed estimator is shown in Fig. 1. The EKF uses the measurements of both voltage, $V(k)$ and current, $I(k)$. The current measurements are used to estimate the polarisation resistance R_{int} by using a fuzzy model and this is one of the inputs of the state estimator for generating the estimated voltage. The voltage modelling error is used for updating the SoC estimator. The proposed EKF based on a fuzzy model will be described on detailed in Sections 3 and 4.

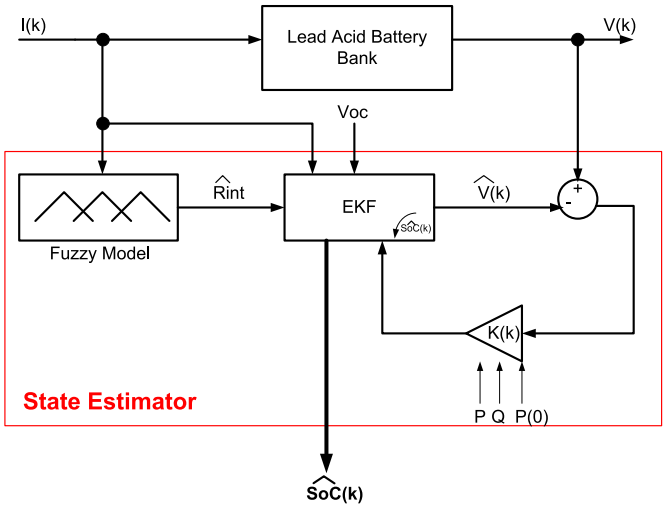

Fig. 1. Scheme of the proposed EKF based on a fuzzy model for SoC estimations.

Two major contributions are highlighted:

- A new fuzzy model for the output voltage of a lead-acid battery bank, which is inspired on the process phenomenology. The polarisation resistance is modelled by a non-linear interpolation (fuzzy based) of a set of available curves obtained experimentally at different operating points of the battery bank. The requirements for experimental data of this model are similar to that required for the identification of classical circuital models of battery banks.
- The proposed EKF is based on a fuzzy model which requires only one internal state in its formulation. This configuration allows an efficient microprocessor implementation, with a reduced number of numerical calculations.

The structure of the paper is as follows. Section 2 presents the lead-acid battery models reported in the literature and their relationship with the problem of lead-acid battery SoC estimation. In Section 3, the fuzzy model proposed by the authors is extensively discussed. The use of an Extended Kalman Filter, based on a fuzzy model, for SoC estimation is presented in Section 4. In Section 5, the design of an experimental system used for system modelling and validation is discussed. In Section 6, the experimental results are shown. Finally, analysis, comments, and further research lines are presented in the conclusions.

2. Classic models for batteries

This work presents a comparison between the performance of the proposed fuzzy model with respect to other well-known battery models (Thevenin, Plett, and Copetti). Thus, we present in this section a brief analysis of all these models, as well as their main features.

2.1. Open circuit voltage curve

There is a well-known relationship between the open-circuit voltage (Voc) and the state-of-charge (SoC) [22,28,29]. Most of the times, this relationship is obtained using an experimental test known as "voltage relaxation": a procedure that basically applies a known discharge profile to the battery for a given period, then forces null discharge current (open circuit) for an appropriate "rest" time (usually an hour), and then measures the (Voc) output voltage [28].

In particular, the Voc-SoC curve in lead-acid batteries can be modelled using a linear-in-the-parameters structure [30], as shown in Eq. (1).

$$\mathrm{Voc}_k = a_n \mathrm{SoC}_k^n + a_{n-1}\mathrm{SoC}_k^{n-1} + \ldots + a_1 \mathrm{SoC}_k + a_0, \tag{1}$$

where $a_i (i = 1, \ldots, n)$ are model parameters. In this model, the SoC is empirically calculated as the integral of the instantaneous current. The discrete model is given by:

$$\mathrm{SoC}_{k+1} = \mathrm{SoC}_k - \frac{T_s}{C_n} I_k, \tag{2}$$

where C_n is the cell nominal capacity (which can be experimentally obtained [22]), T_s is the sampling time, and I_k is the instantaneous discharge current.

2.2. Thevenin circuital equivalent model

The Thevenin circuital equivalent model consists of a controlled voltage source (whose value depends on the SoC), a series *RC* branch, and a series resistance [31–35]. Using this topology and assuming a positive current for battery discharging, a discrete model for the output voltage (as a function of the current) is given by:

$$\begin{aligned} V_k = \mathrm{Voc}_k + [V_{k-1} - \mathrm{Voc}_{k-1}] \cdot e^{\frac{-T_s}{R_0 \cdot C_0}} \\ - \left[R_0 - (R_0 + R_{\mathrm{int}}) \cdot e^{\frac{-T_s}{R_0 C_0}}\right] \cdot I_{k-1} - R_{\mathrm{int}} \cdot I_k, \end{aligned} \tag{3}$$

where Voc_k is obtained from Eq. (1), R_{int} is the polarisation resistance of the battery, C_0 is the capacitance between the electrodes, and R_0 is a non-linear element that represents the contact resistance between the electrodes and electrolyte. For parameter identification purposes, the voltage relaxation test is used for determining the curve SoC–Voc and a test shown in Fig. 2 is used in order to obtain the model resistances and capacitor values.

The Thevenin model can be improved by modifying the polarisation resistance, according to the battery operating point; e.g., assuming different R_{int} for charging and discharging [33].

2.3. Plett model

Plett in Ref. [36] presents a model for a battery bank that depends explicitly on the SoC. In this structure, the output voltage is given by:

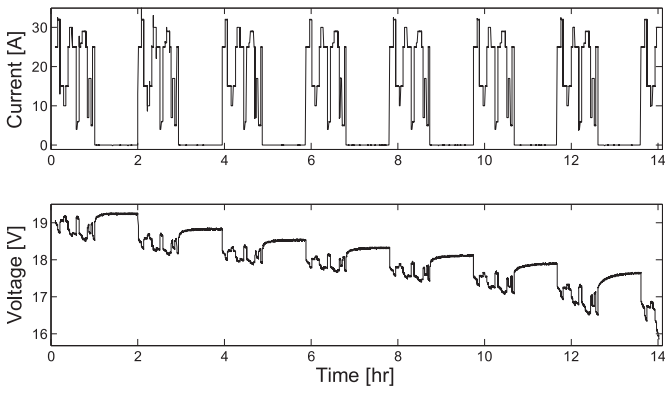

Fig. 2. Training set used for parameter identification purposes.

$$V_k = K_0 - R_{\text{int}} I_k - \frac{K_1}{\text{SoC}_k} - K_2 \text{SoC}_k + K_3 \ln[\text{SoC}_k] + K_4 \ln[1 - \text{SoC}_k], \quad (4)$$

where K_0 represents the polarisation effects, R_{int} is the constant polarisation resistance of the battery storage system and $K_i (i = 1, \ldots, 4)$ are the model coefficients. All the terms associated with K_i represent the relationship between Voc–SoC, and thus the relaxing test is not required as these terms are directly obtained from the experimental tests.

An EKF implementation based on a Plett model has been used in Ref. [37] for the estimation of the SoC in ion-lithium batteries. In this case, only one state variable was included, which is the SoC. This estimator was tested for values higher than 40%. Notice that the Plett model (4) could have numerical errors for SoC near to zero.

2.4. Copetti model

The Copetti model [38,39] considers an equivalent circuit for the battery that contains a constant voltage source and a variable polarisation resistance $R_{\text{int}}(\text{SoC}, I, T)$. The voltage source represents the relationship between Voc and SoC, while R_{int} represents the battery electrochemical effects that oppose to the current flow. The Copetti model describes four operation modes for the battery system; a charging zone, a discharging zone, an overcharging zone and an intermediate zone representing a soft transition between charging/discharging modes. In this work only the discharging zone is studied; therefore, the analytical expression for the output voltage is given by:

$$V_k = [V_{0d} - K_{0d}(1 - \text{SoC}_k)] - \frac{I_k}{C_{10}} \left[\frac{P_{1d}}{1 + I_k^{P_{2d}}} + \frac{P_{3d}}{\text{SoC}_k^{P_{4d}}} + P_{5d} \right] [1 - q_d \Delta T], \quad (5)$$

where $P_{id} (i = 1, \ldots, 5)$ are unknown coefficients associated to the polarisation resistance. C_{10} corresponds to the battery capacity (in AH) for 10 h [39] and q_d relates the model with the temperature variation (ΔT).The term $[V_{0d} - K_{0d}(1 - \text{SoC}_k)]$ models the relationship Voc–SoC. If temperature effects are neglected, the Copetti model equation is:

$$V_k = \text{Voc}_k - \frac{I_k}{C_{10}} \left[\frac{P_{1d}}{1 + I_k^{P_{2d}}} + \frac{P_{3d}}{\text{SoC}_k^{P_{4d}}} + P_{5d} \right]. \quad (6)$$

Also, in this model, the curve Voc–SoC is defined using Eq. (1). Parameters associated with the battery polarisation resistance are identified using data from the training set shown in Fig. 2.

As well as the Plett model, the Copetti model (6) also presents discontinuities when the SoC is near to zero.

3. Fuzzy modelling of lead-acid batteries

The classical models discussed above, have disadvantages (e.g., polarisation resistance is assumed to be constant, numerical errors, discontinuities in the vicinity of SoC near to zero), which could limit their performance in a SoC estimation procedure.

In this section a novel battery model is proposed. It is based on fuzzy system and has the following advantages: i) it offers a non-linear characterization of the battery polarisation resistance, (ii) it requires a limited number of experimental tests for model identification purposes, and (iii) it does not present discontinuities for SoC values in the vicinity of zero.

3.1. Fuzzy model based on rules

Fuzzy logic defines a fuzzy set A, whose elements belong to a discourse universe X as the set of tuples $A = [(x, \mu_A(x))/x \in X]$ where $\mu_A(x)$ is denominated the membership function associated with fuzzy set A. The membership function assigns a membership degree between 0 and 1 to each element of X. The most commonly used membership functions are triangular, trapezoidal and Gaussian shape. Based on this definition, a Takagi & Sugeno fuzzy system corresponds to a set of rules of the form [40]:

$$\text{Rule } j: \text{ If } x \text{ is } A_j \text{ then } y_j = f_j(x, z) \quad (7)$$

$$y(x, z) = \frac{\sum_{j=1}^{r} w_j(x) \cdot y_j(x, z)}{\sum_{j=1}^{r} w_j(x)}, \quad (8)$$

where A_j are the fuzzy sets, f_j is a non-linear function for the rule j, w_j is the activation degree of rule j and r are the number of rules.

3.2. Fuzzy model for a battery bank

The fuzzy model proposed in this work is based on the circuit shown in Fig. 3. It is assumed that the battery output voltage depends on both, the SoC, and the battery current. Temperature variations are not considered in the model, because the battery bank is located in an environment with controlled temperature.

In Fig. 3, the polarisation resistance is modelled as a non-linear function dependant on both the SoC and the discharge current. It is important to note that this equivalent circuit does not consider capacitances. In this regard, it is similar to the equivalent circuits obtained from Plett and Copetti models. Therefore they are used to describe the steady state behaviour of the battery bank.

Based on Fig. 3, the fuzzy model discrete equation is given by:

$$V_k = \text{Voc}_k - I_k \cdot \widehat{R}_{\text{int}}(\text{SoC}_k, I_k), \quad (9)$$

where the voltage source Voc_k is obtained from Eq. (1). Therefore, the values of the proposed polarisation resistance can be obtained using Eq. (9), i.e.:

$$\widehat{R}_{\text{int}}(\text{SoC}_k, I_k) = \frac{\text{Voc}_k - V_k}{I_k}. \quad (10)$$

To obtain the polarisation resistance of the proposed model (see Fig. 3), experimental tests at fixed discharge current levels are performed (see Fig. 2). Fig. 4 shows the computed values of resistances in function of SoC, using Eq. (10) and current values of 10 A, 15 A, 25 A, 32 A, together with the corresponding output voltage measurements V_k. To calculate the equivalent polarisation resistance for any value of discharge current within the operating range, the proposed fuzzy model interpolates between the resistance curves depicted in Fig. 4. Thus, the structure for the proposed fuzzy model and its rules for the calculation of $\widehat{R}_{\text{int}}(\text{SoC}_k, I_k)$ are:

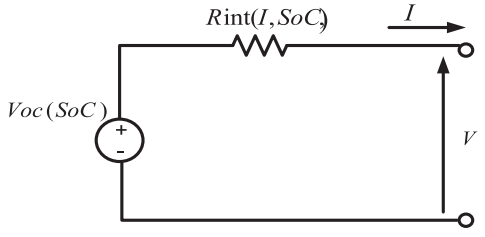

Fig. 3. Circuital representation of the fuzzy model.

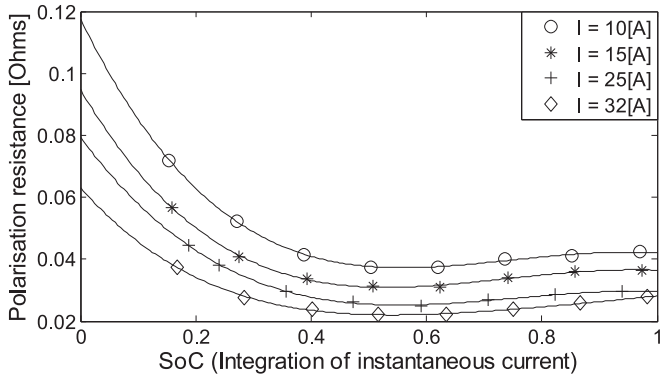

Fig. 4. Polarisation resistance values at different current levels.

$$\text{Rule } j: \text{ If } I_k \text{ is } A_{I_j,j} \quad \text{then } \widehat{R}_{\text{int}_j} = f_j(\text{SoC}_k), \tag{11}$$

$$\widehat{R}_{\text{int}}(\text{SoC}_k, I_k) = \frac{\sum_{j=1}^{r} w_j(I_k)\cdot f_j(\text{SoC}_k)}{\sum_{j=1}^{r} w_j(I_k)}, \tag{12}$$

where w_j is the activation degree of rule j (in this case, equal to the membership degree to the fuzzy set $A_{I_j,j}$) and f_j is a non-linear function adjusted for the resistance values $\widehat{R}_{\text{int}_j}$ in function of SoC_k at a fixed level of the current I_j (see curves from Fig. 4). The fuzzy sets are obtained from the experimental data (Fig. 4) and they are shown in Fig. 5.

Gaussian membership functions for the fuzzy sets $A_{I_j,j}$ are proposed in this work. Gaussian membership functions have been selected because they only require two parameters (mean value and standard deviation) to be completely defined. In this particular case, the mean value of these functions is defined as I_j, and the standard deviation is selected to minimise the model mean square error.

Finally, it is important to mention that the fuzzy model implementation requires similar experimental data size than that required for the implementation of Thevenin and Copetti models.

4. Extended Kalman filter based on fuzzy models for SoC estimation

The proposed fuzzy model is important for the estimation of the SoC using the Extended Kalman Filter algorithm. The classic formulation of the EKF considers a non-linear stochastic system that can be represented by the following discrete time state space equations [7]:

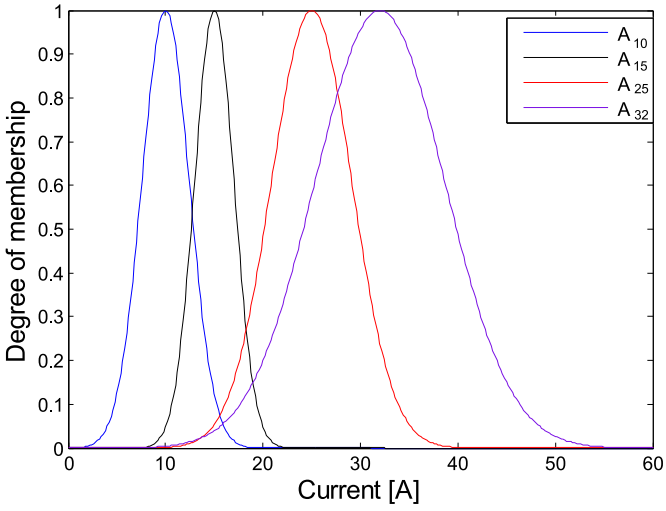

Fig. 5. Fuzzy sets for current values.

$$x_k = f(x_{k-1}, u_{k-1}) + \omega_k \tag{13}$$

$$y_k = h(x_k, u_k) + v_k, \tag{14}$$

where $x_k \varepsilon R^n$ is the unknown state vector, $u_k \varepsilon R^r$ are known process inputs, and $y_k \varepsilon R^m$ are observation outputs. Process and measurement noises are denoted by ω_k and v_k (Gaussian), with variances Q and R respectively; while $f(\cdot)$ and $h(\cdot)$ are non-linear functions that characterise the state transition and measurement equations, in that order.

The EKF has the same structure of the well-known linear Kalman filter [41]. Eqs. (13) and (14) are used to characterise the non-linear state transition equation. These equations are linearised using the Taylor expansion, and only selecting its first term. Thus, the expectation of the estimate state probability density function (PDF) is given by:

$$\widehat{x}_{k/k-1} = f(\widehat{x}_k, u_k) + \omega_k \tag{15}$$

The $P_{k/k-1}$ covariance matrix is obtained by calculating a derivative respect to $\widehat{x}_{k/k-1}$ as:

$$A_{k-1} = \left.\frac{\partial f}{\partial x_{k-1}}\right|_{\widehat{x}_{k/k-1}, u_{k-1}} \tag{16}$$

$$P_{k/k-1} = A_{k-1} P_{k-1/k-1} A_{k-1}^T + Q. \tag{17}$$

Once the prediction step is completed, the following equations are computed:

$$\tilde{y}_k = y_k - h\left(\widehat{x}_{k/k-1}, u_k\right) \tag{18}$$

$$S_{k/k-1} = C_k P_{k/k-1} C_k^T + R, \tag{19}$$

where C_k is given by:

$$C_k = \left.\frac{\partial h}{\partial x_k}\right|_{\widehat{x}_{k/k-1}} \tag{20}$$

If (20) is evaluated at the prior state estimate $\widehat{x}_{k/k-1}$, then the Kalman gain K_k is computed as in Eq. (21). This Kalman gain is afterwards used in Eq. (22) to generate the posterior estimate $\widehat{x}_{k/k}$. Finally, the error covariance matrix $P_{k/k}$ is calculated using Eq. (23).

$$K_k = P_{k/k-1} C_k^T \left(C_k P_{k/k-1} C_k^T + R\right)^{-1} \tag{21}$$

$$\widehat{x}_{k/k} = \widehat{x}_{k/k-1} + K_k\left(y_k - h\left(\widehat{x}_{k/k-1}, u_k\right)\right) \tag{22}$$

$$P_{k/k} = (I - K_k C_k) P_{k/k-1} \tag{23}$$

4.1. EKF based on a fuzzy model

The state space model that is proposed in this implementation uses Eq. (2), which relates the SoC with the integral of the instantaneous current, as the state equation and the output voltage of the proposed model (9) as the observation equation, respectively:

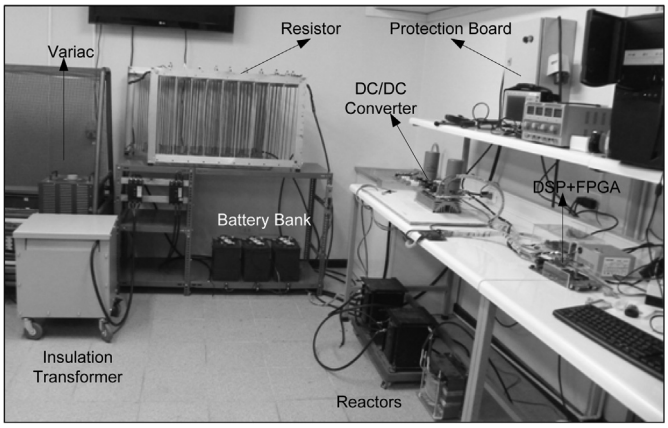

Fig. 6. Setup of the experimental system.

$$\widehat{\mathrm{SoC}}_{k/k-1} = \widehat{\mathrm{SoC}}_{k-1/k-1} - \frac{T_s I_{k-1}}{C_n} \tag{24}$$

$$\widehat{V}_{k/k-1} = V_{\mathrm{oc}}\left(\widehat{\mathrm{SoC}}_{k/k-1}\right) - I_k \widehat{R}_{\mathrm{int}}\left(\widehat{\mathrm{SoC}}_{k/k-1}, I_k\right). \tag{25}$$

Therefore, the estimation of the SoC is obtained using the EKF (see Eqs. (15)–(23)), which is based on the model described by Eqs. (9)–(12). Thus the SoC is estimated using:

$$\widehat{\mathrm{SoC}}_k = \widehat{\mathrm{SoC}}_{k/k-1} + K_k \cdot \left[V_k - \widehat{V}_{k/k-1}\right] \tag{26}$$

$$K_k = P_{k/k-1} \cdot C_k^T \cdot \left[C_k \cdot P_{k/k-1} \cdot C_k^T + R\right]^{-1} \tag{27}$$

$$P_k = [I - K_k \cdot C_k] \cdot P_{k/k-1}, \tag{28}$$

where C_k is the first term in a Taylor expansion of the fuzzy model (see Eqs. (9)–(12)):

$$C_k = \left.\frac{\partial V_k}{\partial \mathrm{SoC}}\right|_{\widehat{\mathrm{SoC}}_{k/k-1}} = \left.\frac{\partial V_{\mathrm{OC}}}{\partial \mathrm{SoC}}\right|_{\widehat{\mathrm{SoC}}_{k/k-1}} - \frac{I_k}{\sum_{j=1}^{r} w_j(I_k)} \left(\sum_{j=1}^{r} w_j(I_k) \cdot \left.\frac{\partial f_j(\mathrm{SoC}_k)}{\partial \mathrm{SoC}_k}\right|_{\widehat{\mathrm{SoC}}_{k/k-1}} \right) \tag{29}$$

and:

$$P_{k/k-1} = P_{k-1/k-1} + Q. \tag{30}$$

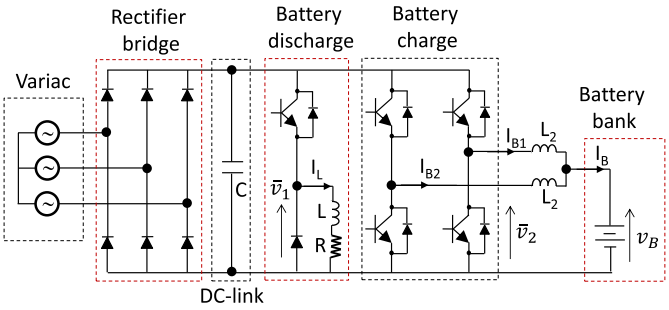

Fig. 7. Experimental system topology.

Table 1
Parameters of the experimental system.

Nominal power of the experimental system	4 kW
Inductance for battery charging	30 mH
Battery bank	3 Trojan T-105. 18 V in total (nominal)
Nominal capacity	185 Ah
Switching frequency	4 KHz
Inductance and resistance for battery discharging	15 mH, 1 Ω
Control platform	DSK 6713, FPGA ACTEL A3P400
DC-link capacitance	2 Parallel-connected capacitors of 75 V, 33,000 μF each.

In summary, the EKF described is based on a new fuzzy model which it is used as the observation equation with just one state defined by the SoC. Thus, the resulting algorithm is efficient and entails low computational burden when programmed on a microprocessor.

5. Experimental system

In this work an experimental system has been designed and implemented in order to

- Validate the proposed methodology using experimental data, obtained by discharging a lead-acid battery bank. The same system is used to charge the batteries according to the charging profile recommended by the manufacturers.
- Experimental data has been used to comparate the performance of the proposed model respect to the performance of other models reported in the literature.
- Experimental data has been used for comparate the performance of the SoC estimator based on the fuzzy model and a SoC estimator based on a conventional model.

The experimental prototype is shown in Fig. 6 and its topology in Fig. 7. This converter topology is relatively inexpensive and

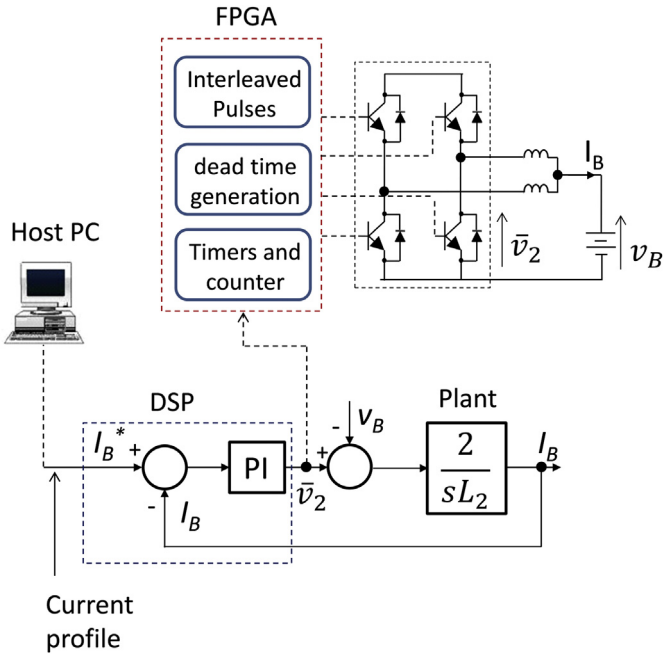

Fig. 8. Control system and associate hardware for battery charging.

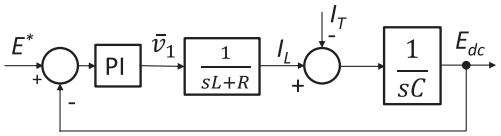

Fig. 9. Control system for battery bank discharging.

simple to implement. Information about the parameters of the experimental system is provided in Table 1.

The input to the battery charging/discharging system (see Fig. 7), is a variable output transformer designed to supply a voltage of 40 V, 100 A. A bridge rectifier is required to feed a DC-link capacitor bank of 66,000 μF. This DC-link is connected to two blocks labelled "Battery charge" and "Battery discharge". A Digital Signal Processor (DSP), Texas Instrument DSK 6713 is used to control the whole system. As shown in Fig. 8 this DSP platform is connected to a host computer. An FPGA based board is utilised to generate the IGBT switching pulses and for protection purposes. An additional board with 10 ADs channels of 14 bits, 1 μs of conversion time is provided. Hall-effect transducers are used to measure the DC-link voltages, the voltage of the battery bank, the currents (I_{B1}, I_{B2}) and the current in the resistance where the energy is dissipated when the batteries are being discharged. The control systems required to charge and discharge the battery bank are discussed below.

5.1. Control system for charging the battery bank

To charge the battery bank, the control system and associate hardware shown in Fig. 8 have been implemented in this work. To operate with currents close to 100 A with minimum ripple in the battery bank, two inductors are used with interleaved switching signals. The switching frequency used to control the system is 4 kHz for a sampling time (in the DSP implementation) of 250 μs. The host computer is also used to acquire and store intermediate data, with a sampling time of 1 s. This time is considered appropriate considering the relatively slow variation of the current profile. A MATLAB® interface has been implemented to acquire and process the data sent from the DSP.

The reference charging current (see bottom left side of Fig. 8) corresponds to a profile which is stored in the host computer. A PI controller regulates the DC component of the voltage (see $\bar{v}_2$ in Figs. 7 and 8) at the actuator output. Assuming that the two inductors/IGBT legs are identical, the battery current I_B is obtained as:

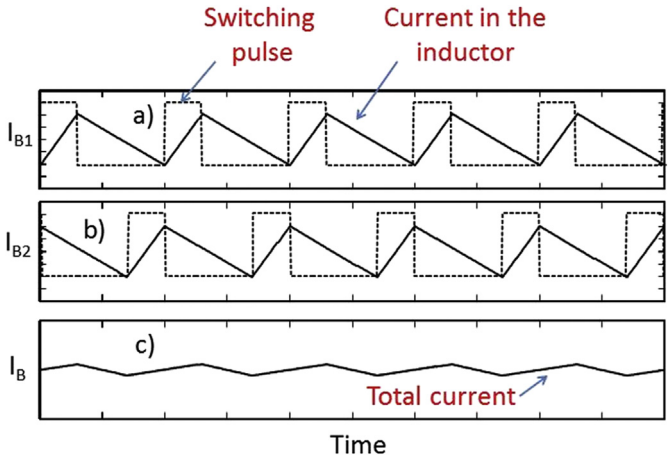

Fig. 10. Interleaved operation of the two legs used for battery charging.

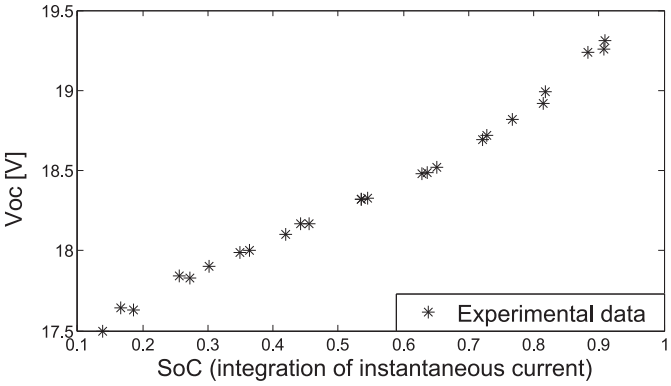

Fig. 11. VoC–SoC relation.

$$I_B = \frac{2}{sL_2}(\bar{v}_2 - v_B). \tag{31}$$

Using Eq. (31) and root-locus, it is relatively simple to design a current control system. For this application a natural frequency of $\omega_n \approx 20$ Hz and damping factor $\zeta = 0.8$ are used. This natural frequency is considered sufficient for this application.

5.2. Control system for discharging the battery bank

To discharge the battery bank, the reference current regulated by the control system of Fig. 8 is negative (i.e. $I_B^* < 0$). Therefore in steady state $\bar{v}_2 < v_B$ and the actuator is operated as a boost converter, increasing the DC-link voltage E_{dc}.

When the DC-link voltage is above a given value, the control system shown in Fig. 9 is activated. A PI controller is used to regulate the DC-voltage $\bar{v}_1$ which is applied to the load composed of an inductor L and a resistance R (see "battery discharge" block in Fig. 7). Neglecting the losses, in steady state the PI controller drives the current I_L to the value:

$$I_L = I_T = \frac{v_B I_B}{E^*}, \tag{32}$$

where I_T is the total current provided by the battery bank to the DC-link.

Considering the large DC-link capacitance, the natural frequency of this control loop is $\omega_n \approx 5$ Hz, with a damping coefficient of $\zeta \approx 0.8$.

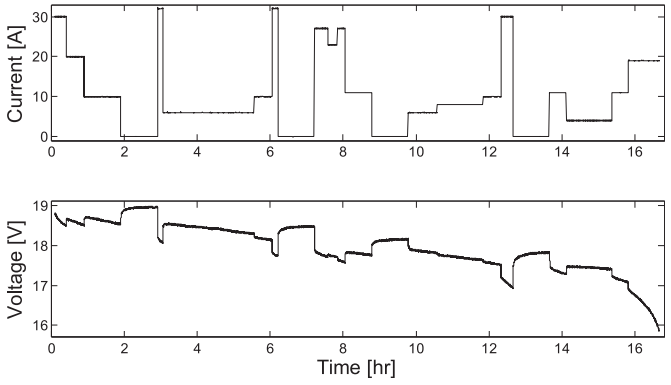

Fig. 12. Validation set 1.

5.3. Interleaved operation

In order to charge and discharge the battery bank, with a relatively high current and low ripple, the two inductors available for this work were connected for interleaved operation. This allows a considerable reduction in the current ripple, maintaining the inductor currents below the rating values. For interleaved operation the FPGA was programmed to switch each IGBT with identical duty cycle but with a phase shift of 180°.

The waveforms are shown in Fig. 10 where the switching pulses and its associated inductor currents are displayed in Fig. 10a and b. Notice that the DC current components are identical in both inductors, however part of the harmonic distortion is eliminated when the currents I_{B1} and I_{B2} are added. More information about interleaved operation of current control system is elsewhere [42].

6. Experimental evaluation of the model performance

In this section data from experimental system discussed in Section 5 is used to identify the parameter of all the models presented in Section 2. These are:

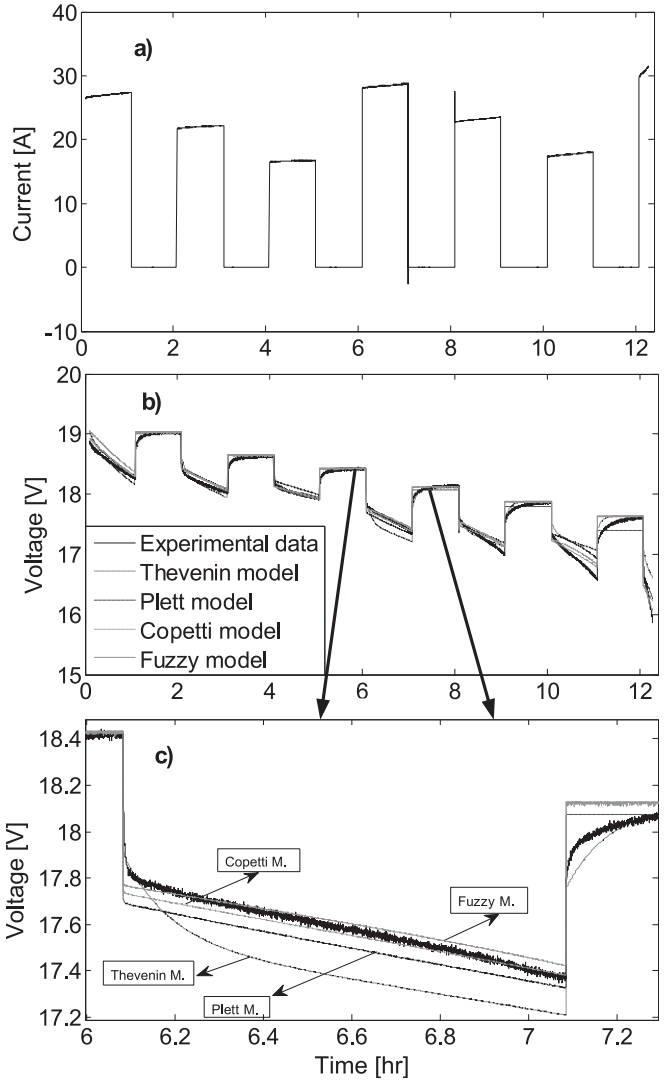

Fig. 13. a) Validation set 2, b) model comparison in validation set 2, c) model comparison in validation set 2, zoom for a time period.

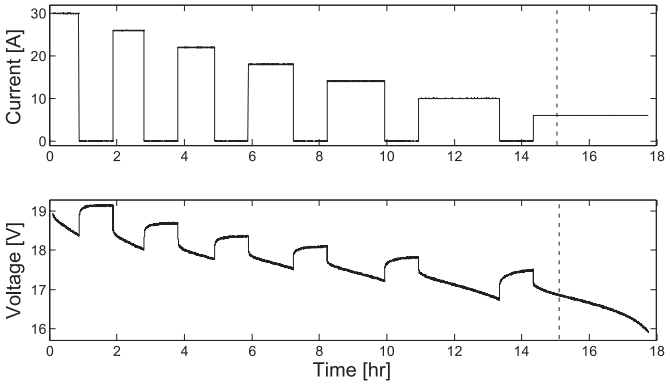

Fig. 14. Validation set 3. The subset 3 is defined from $t = 0$ until $t \approx 15$ (see dotted line).

- Open circuit voltage curve
- Thevenin model
- Plett model
- Copetti model
- Proposed fuzzy model

For this evaluation the parameters of Eq. (1) have been identified using the relaxation tests described in Section 2.1 and genetic algorithms [43]. This Voc–SoC curve was obtained experimentally and it is shown in Fig. 11. This relationship can be mathematically written as (see Eq. (1)):

$$\mathrm{Voc}_k = 3.755\mathrm{SoC}_k^3 - 5.059\mathrm{SoC}_k^2 + 3.959\mathrm{SoC}_k + 17.064 \tag{33}$$

As described in Eq. (2), the SoC is calculated as the integral of the instantaneous current with a sampling time of $T_s = 1$ s and nominal capacity (C_n) equal to 165 Ah, which is obtained from a capacity experimental test at 10 A.

The comparative analysis of model performances is generated in terms of the Root Mean Square Error (RMSE), which is given by:

$$\mathrm{RMSE} = \sqrt{\frac{\sum_{i=1}^{N}\left(V_i - \widehat{V}_i\right)^2}{N}}, \tag{34}$$

where N is the number of samples (from experimental data), V_i is the actual output voltage (obtained using the experimental system of Section 5) and $\widehat{V}_i$ is the estimated output voltage obtained from the battery bank model considered.

6.1. Parameter identification

The data used in the training and validation sets are obtained from battery discharging profiles programmed in the DSP controlling the experimental platform. Notice that temperature effects in this work were not considered since the experimental setup was allocated in a room with constant temperature. The parameters

Table 2
RMSE performance models on validation sets.

Models	Set #1 RMSE [V]	Set #2 RMSE [V]	Set #3 RMSE [V]	Set #3* RMSE [V]
Thevenin	0.1548	0.1259	0.2457	0.1584
Plett	0.1174	0.1087	2.8840	0.2096
Copetti	0.0717	0.0978	1.7005	0.0644
Fuzzy rules	0.0819	0.0866	0.0753	0.0589

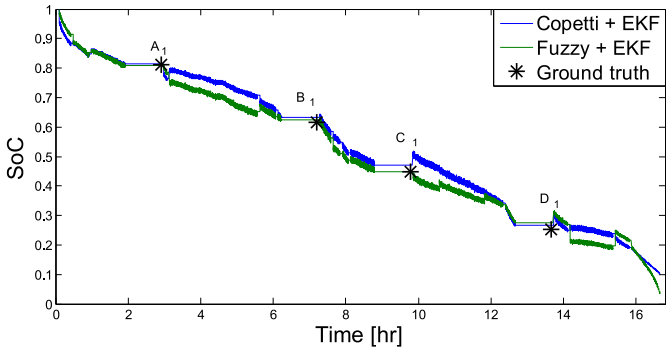

Fig. 15. EKF estimators based on Copetti and fuzzy models in validation set 1.

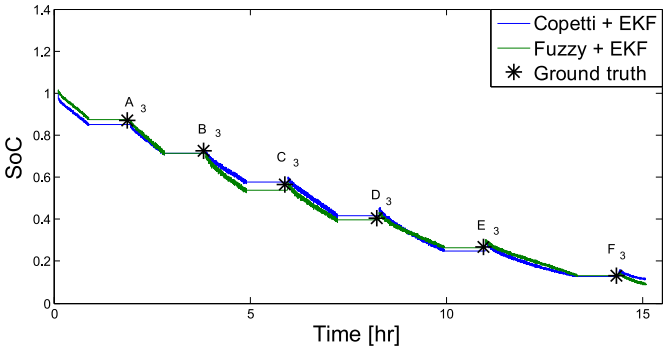

Fig. 17. EKF estimators based on Copetti and fuzzy models in validation set 3.

required in the Thevenin, Copetti, Plett, and fuzzy models are identified using the training sets shown in Fig. 2.

Using the discrete expression defined in Eq. (3) the parameters of the Thevenin model are estimated as: $R_{\text{int}} = 0.019\ \Omega$; $C_0 = 28{,}747.99$ F and $R_0 = 0.013\ \Omega$.

$$V_k = \text{Voc}_k + [V_{k-1} - \text{Voc}_{k-1}]\cdot e^{\frac{-1}{0.013\cdot 28747.99}} - \left[0.013 - (0.013 + 0.019)\cdot e^{\frac{-1}{0.013\cdot 28747.99}}\right]\cdot I_{k-1} - 0.019\cdot I_k, \tag{35}$$

The parameters of the Plett model (see (4)) are estimated as: $K_0 = 15.33$, $K_1 = 0.471$, $K_2 = -4.408$, $K_3 = -2.249$, $K_4 = -0.085$ and $R_{\text{int}} = 0.026\ \Omega$.

$$V_k = 15.33 - 0.026 I_k - \frac{0.471}{\text{SoC}_k} + 4.408\text{SoC}_k - 2.249\ln[\text{SoC}_k] - 0.085\ln[1-\text{SoC}_k], \tag{36}$$

The parameters of the Copetti model described in Eq. (6) are estimated as: $C_{10} = 138.003$ Ah, $P_{1d} = 49.246$, $P_{2d} = 1.089$, $P_{3d} = 0.063$, $P_{4d} = 2.082$ and $P_{5d} = 1.986$.

$$V_k = \text{Voc}_k - \frac{I_k}{138.003}\left[\frac{49.246}{1 + I_k^{1.089}} + \frac{0.063}{\text{SoC}_k^{2.082}} + 1.986\right], \tag{37}$$

The fuzzy model rules obtained (based on the methodology discussed in Section 3.2) are:

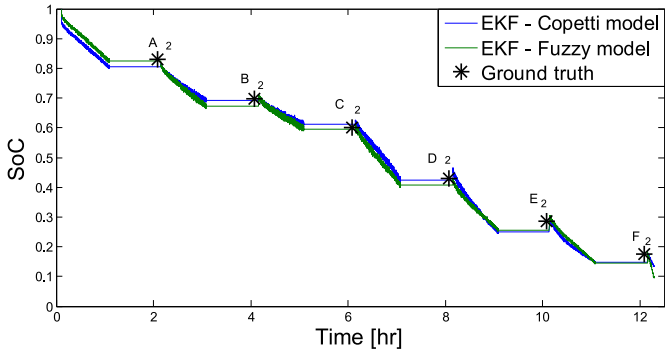

Fig. 16. EKF estimators based on Copetti and fuzzy models in validation set 2.

$$\text{Rule 1: If } I_k \text{ is } A_{10,1} \text{ then } \widehat{R}_{\text{int}_1} = 0.070\text{SoC}_k^4 - 0.382\text{SoC}_k^3 + 0.619\text{SoC}_k^2 - 0.383\text{SoC}_k + 0.118$$

$$\text{Rule 2: If } I_k \text{ is } A_{15,2} \text{ then } \widehat{R}_{\text{int}_2} = 0.067\text{SoC}_k^4 - 0.338\text{SoC}_k^3 + 0.529\text{SoC}_k^2 - 0.316\text{SoC}_k + 0.095$$

$$\text{Rule 3: If } I_k \text{ is } A_{25,3} \text{ then } \widehat{R}_{\text{int}_3} = 0.031\text{SoC}^4 - 0.219\text{SoC}_k^3 + 0.391\text{SoC}_k^2 - 0.253\text{SoC}_k + 0.079$$

$$\text{Rule 4: If } I_k \text{ is } A_{32,4} \text{ then } \widehat{R}_{\text{int}_4} = 0.083\text{SoC}^4 - 0.284\text{SoC}_k^3 + 0.374\text{SoC}_k^2 - 0.208\text{SoC}_k + 0.063$$

Fig. 5 shows the membership functions of the fuzzy sets $A_{l_j,j}$. Therefore using $A_{l_j,j}$ (see Fig. 5) and Eq. (12), $\widehat{R}_{\text{int}}(\text{SoC}_k, I_k)$ is obtained as model output.

6.2. Evaluating of the model performance using the RMSE criterion

In this work, three separated sets are used for validating purposes. These validation sets are not correlated with the training sets (see Fig. 2). A short description of each validation sets is shown below:

Validation set #1 (Fig. 12). It includes battery discharge profiles obtained in different operating points. This validation set has been designed to use instantaneous current levels different to those of the training set.

Validation set #2 (Fig. 13a). It includes data from a battery discharging current profile with three different levels of constant power. This validation set has been designed to emulate the consumption of electric vehicles operating at cruise speed [22].

Table 3
Performance indices on validation set 1.

Points	EKF-Copetti [%]		EKF-fuzzy rules [%]	
	I_{1k}^C	I_{2k}^C	I_{1k}^F	I_{2k}^F
A_1	0.40	1.19	0.17	0.47
B_1	2.76	4.31	1.26	1.62
C_1	4.93	4.68	0.17	0.18
D_1	5.76	6.11	9.41	10.86

Table 4
Performance indices on validation set 2.

Points	EFK-Copetti [%]		EFK-fuzzy rules [%]	
	I^C_{1k}	I^C_{2k}	I^F_{1k}	I^F_{2k}
A_2	2.91	8.68	0.56	1.53
B_2	0.77	1.52	3.51	5.68
C_2	1.77	2.55	0.63	0.79
D_2	1.63	1.67	5.49	6.62
E_2	13.0	15.6	10.1	13.3
F_2	15.2	27.2	17.5	19.5

Validation set #3 (Fig. 14). It is generated by using a current profile that consists of periods where the battery discharges 30 Ah (using different discharge currents each time) with interspersed periods of relaxation. This validation set has been designed to test the performance of the model with different discharging current.

Notice that at the beginning of each experimental test, the value of the SoC is 100%. Also, it must be noted that the charging profile current recommended by the manufacturer, includes two stages. In the first stage, the battery is charged at a constant current of 25 A; while in the second stage constant voltage is applied to the battery until the injected current is less than or equal to 5 A.

Table 2 shows the performance indices (RMSE) for Thevenin, Copetti, Plett, and fuzzy model, using the three aforementioned validation sets. Also, a subset of the set #3 (set #3*) includes only SoC values between 0.1 and 1 to avoid the discontinuities that affect both Plett and Copetti models. Fig. 13b and c shows the results of the models for the validation set #2.

From Table 2, it is concluded that the best results in terms of the RMSE index are obtained with the Copetti and fuzzy models. Except in set #1, the proposed fuzzy model behaves consistently better than the other three circuital models. The proposed fuzzy model has a slightly worse performance with validation set #1, because this model has not been trained to operate with low discharging currents (see Fig. 4). In all the cases where the proposed fuzzy model has been adequately trained, the fuzzy model outperformed the others models including the Copetti model.

Considering the results obtained using the validation tests, the two models with the best performance are used in the next section to investigate the performance of a SoC estimation algorithm based on an EKF.

7. EKF estimators

To evaluate the performance of the EKF SoC estimators, the following indices are defined

$$I_{1k} = \frac{\left|\widehat{\mathrm{SoC}}_k - \mathrm{SoC}_k\right|}{\mathrm{SoC}_k} \cdot 100\% \tag{38}$$

Table 5
Performance indices on validation set 3.

Points	EFK-Copetti [%]		EFK-fuzzy rules [%]	
	I^C_{1k}	I^C_{2k}	I^F_{1k}	I^F_{2k}
A_3	2.38	8.32	0.46	1.53
B_3	1.95	4.13	1.89	3.32
C_3	2.70	3.54	4.65	5.61
D_3	2.63	2.47	2.48	2.82
E_3	6.47	6.08	0.45	0.48
F_3	1.47	1.80	2.47	1.87

Table 6
Convergence times in validation set 1 using EKF estimators.

Initial SoC	Error	EKF-Copetti [s]	EKF-fuzzy rules [s]
0.1	90%	4.6	2.9
0.3	70%	1.8	2.9
0.5	50%	2.7	2.5
0.7	30%	2.0	2.6

Table 7
Convergence times in validation set 2 using EKF estimators.

Initial SoC	Error	EFK-Copetti [s]	EFK-fuzzy rules [s]
0.1	90%	4.6	3.1
0.3	70%	1.8	2.9
0.5	50%	2.7	2.5
0.7	30%	2.0	2.5

$$I_{2k} = \frac{\left|\widehat{\mathrm{SoC}}_k - \mathrm{SoC}_k\right|}{2\sqrt{P_{k/k}}} \cdot 100\%, \tag{39}$$

where $P_{k/k}$ is the EKF covariance matrix (evaluated at the sampling instant k). The index of Eq. (38) describes the error between the estimated value $\widehat{SoC}_k$ and the real value SoC_k.

The index of Eq. (39) is based on the error of the estimated SoC value respect to the length of the confidence interval at 95%. If both indices are below a given threshold, the SoC estimation would be close to its actual value.

The R (covariance of measurement noise) and Q (covariance of process noise) matrices required in the Kalman filter (see Eqs. (17)–(19)) were obtained using the data sheets of the corresponding sensors, where information about the typical noise introduced to the measurements is stated. For the voltage transducer, there is an error ≈0.9% with a noise variance of $\sigma^2 = (0.9/2)^2 = 0.2025$, then $R = 0.2$ is used.

For determining the lower bound of R, the model error has to be higher that the input variable error. For this application, the instantaneous current is the input, and the associated sensor error is 1%. Then the variance is: $\sigma^2 = (1/2)^2 = 0.25$. As the matrix R should be higher than 0.25 then $Q = 0.5$ is selected. Thus, the initial covariance matrix is $P_o = 0.5$.

7.1. Performance of the EKF estimators based on Copetti and fuzzy models

SoC EKF estimators based on both Copetti and fuzzy models have been evaluated using the aforementioned validation sets. Figs. 15–17 show the SoC ground truth (values that are considered as actual SoC) and the results of EKF estimators, assuming the battery is fully charged at the beginning of the experiment. SoC ground truth was computed off-line by considering both the integral of the instantaneous current and battery open circuit voltage after each relaxing period.

Table 8
Convergence times in validation set 3 using EKF estimators.

Initial SoC	Error	EKF-Copetti [s]	EKF-fuzzy rules [s]
0.1	90%	4.7	3.4
0.3	70%	1.8	2.9
0.5	50%	2.8	2.7
0.7	30%	2.3	2.7

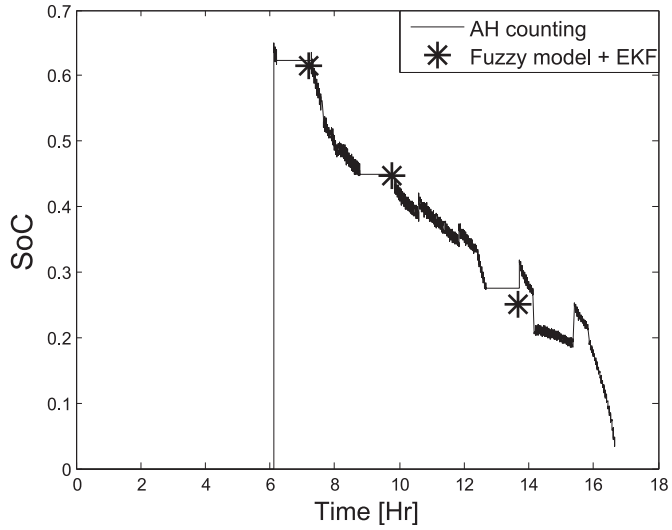

Fig. 18. Performance SoC estimator in validation set 1 (estimator is turn on in $t = 6$ h).

Tables 3–5 show the values obtained by evaluating the performance indices of Eqs. (38) and (39) using the experimental data depicted in Figs. 15–17. From Figs. 16 and 17, it can be noted that the proposed estimators provide outputs that are consistent with the ground truth that was acquired in an off-line manner (validation sets #2 and #3).

According to what it was presented in Section 6.2, the estimator accuracy is directly affected by the fact that the fuzzy model was trained using data with battery discharge currents higher than 10 A. This issue becomes evident when analysing the estimator performance using set #1 (see Fig. 15). Also, the EKF estimators are turned off during the relaxation periods; i.e., when the discharge current is null.

Additionally, the estimator performance is evaluated using three validation sets for different values of the initial conditions of SoC (30%, 50%, 70% and 90% of the initial SoC errors). Validation tests are used to obtain the convergence times of both EKF estimators (Copetti and fuzzy). The convergence time is defined as the time t_c when the estimator output gets into a predefined zone, based on an upper and a lower band without leaving this zone again for $t > t_c$.

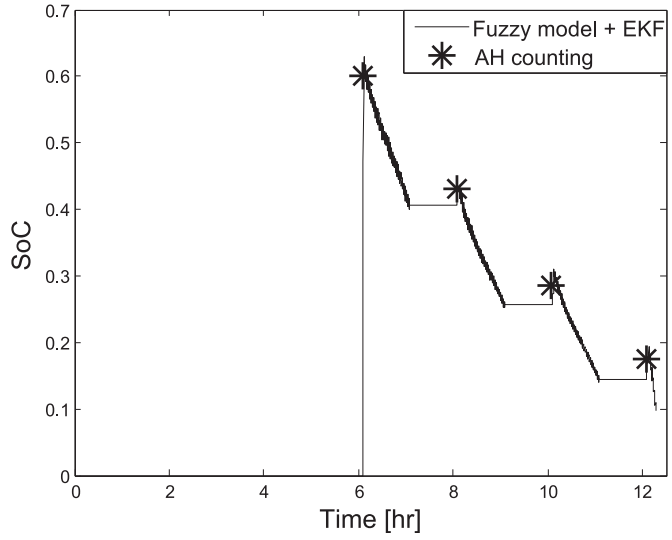

Fig. 19. Performance SoC estimator in validation set 2 (estimator is turn on in $t = 6$ h).

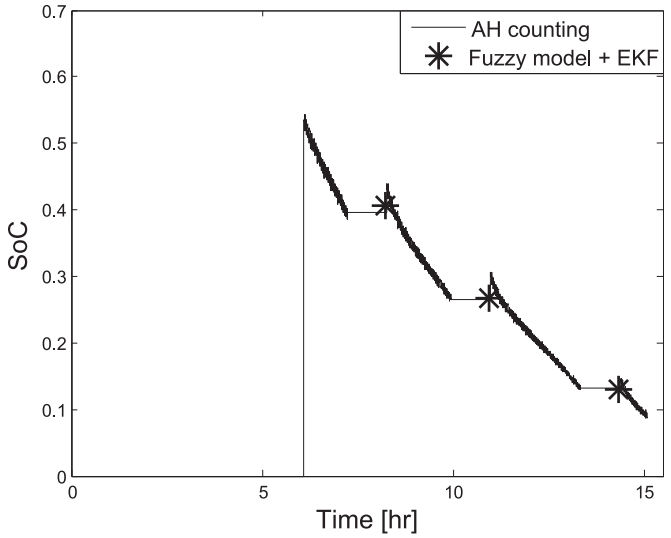

Fig. 20. Performance SoC estimator in validation set 3 (estimator is turn on in $t = 6$ h).

Tables 6–8 show the convergence times for both estimators. From the information displayed in the aforementioned tables, we conclude that a fast convergence for both EKF estimators is achieved. Also, note that convergence times are influenced by the initial value assumed for the SoC.

Finally, Figs. 18–20 show the estimator performance considering all three validation sets. In these experiments, the proposed SoC estimator is turned on after the battery bank has been discharged for at least six consecutive hours approx. As shown in Figs. 18–20, the estimator converges to the SoC ground truth values after few iterations.

8. Conclusions

In this paper, a new fuzzy model for the estimation of lead-acid battery bank SoCs has been presented. The fuzzy rules are based on the battery polarisation resistance behaviour at different current levels.

The fuzzy model has been compared with several conventional models using the *RMS* error as goodness factor. In all the cases its performance was better than that obtained by the conventional models discussed in this work. Moreover, the proposed SoC estimator does not have any numerical issues or mathematical discontinuities when the battery SoC is near to zero. This is certainly an advantage of the proposed algorithm when compared to the Plett and Copetti models.

In this work it has also been observed that the performance of the models is improved by modelling the battery polarisation resistance as a non-linear resistor whose value is dependant on the SoC value and the discharging current. This is an additional advantage of the proposed model when compared to other algorithms where a fixed polarisation resistance value is assumed.

The fast converge of the proposed EKF estimator based on a fuzzy model, allows on-line implementation. Moreover the fuzzy model discussed in this work has converged to the correct SoC value even when the initial SoC value has been very badly estimated.

Acknowledgements

This work has been partially supported by FONDECYT project 1140775 and the Complex Engineering Systems Institute (ICM: P-

05-004-F, CONICYT: FBO16). The support of the Conicyt scholarship programme for postgraduated studies, is also acknowledged.

References

[1] R. Palma-Behnke, C. Benavides, F. Lanas, B. Severino, L. Reyes, J. Llanos, D. Sáez, IEEE Trans. Smart Grid 4 (2) (2013) 996–1006.
[2] V. Agarwal, K. Uthaichana, R.A. DeCarlo, L.H. Tsoukalas, IEEE Trans. Energy Convers. 25 (3) (2010) 821–835.
[3] A. Purvins, M. Sumner, J. Power Sources (242) (2013) 742–755.
[4] A. Salkind, C. Fennie, P. Singh, T. Atwater, D. Reisner, J. Power Sources 80 (1–2) (1999) 293–300.
[5] M. Charkhgard, M. Farrokhi, IEEE Trans. Ind. Electron. 57 (12) (2010) 4178–4187.
[6] B. Saha, K. Goebel, in: Annual Conference of the Prognostics and Health Management Society, San Diego, CA, 2009.
[7] D. Vinh Do, C. Forgez, K. El-Kadri-Benkara, G. Friedrich, IEEE Trans. Veh. Technol. 58 (8) (2009) 3930–3937.
[8] B. Olivares, M. Cerda, M. Orchard, J.F. Silva, IEEE Trans. Instrum. Meas. 62 (2) (2013) 364–376.
[9] B. Pattipati, C. Sankavaram, K. Pattipati, IEEE Trans. Syst. Man Cybern. Part C Appl. Rev. 41 (6) (2011) 869–884.
[10] D. Cadar, D. Petreus, C. Orian, in: 15th International Symposium for Design and Technology of Electronics Packages (SIITME) 2009, 2009, pp. 257–260.
[11] S. Qingsheng, Z. Chenghui, C. Naxin, Z. Xiaoping, in: 29th Chinese Control Conference (CCC) 2010, 2010, pp. 5999–6003.
[12] Z. Di, M. Yan, B. Qing-Wen, in: 30th Chinese Control Conference (CCC) 2011, 2011, pp. 6256–6260.
[13] S. Lee, J. Kim, J. Lee, B. Cho, J. Power Sources 185 (2) (2008) 1367–1373.
[14] X. Tang, X. Mao, J. Lin, B. Koch, in: American Control Conference (ACC) 2011, 2011.
[15] L. Ran, W. Haiying, L. Gechen, in: 5th IEEE Conference on Industrial Electronics and Applications (ICIEA), 2010.
[16] M. Dalal, J. Ma, D. He, Proc. Inst. Mech. Eng. Part O J. Risk Reliab. (2011) 81–90.
[17] P. Singh, C. Fennie, D. Reisner, J. Power Sources 139 (2) (2004) 322–333.
[18] A. Zenati, P. Desprez, H. Razik, in: 36th Annual Conference on IEEE Industrial Electronics Society EICON 2010, Glendale, AZ, 2010.
[19] P. Singh, R. Vinjamuri, X. Wang, D. Reisner, J. Power Sources 162 (2) (2006) 829–836.
[20] S. Malkhandi, Eng. Appl. Artif. Intell. 19 (5) (2006) 479–485.
[21] P. Singh, A. Nallanchakravarthula, in: Proceedings of the 13th International Conference on Intelligent Systems Application to Power Systems, Arlington, VA, 2005.
[22] U.S. Department of Energy, PNGV Battery Test Manual, Revision 3, DOE/ID-10597, 2001.
[23] C. Cai, D. Du, Z. Liu, in: The 12th IEEE International Conference on FUZZ '03, 2003.
[24] I. Li, W. Wang, S. Su, Y. Lee, IEEE Trans. Energy Convers. 22 (3) (2007) 697–708.
[25] S. Santhanagopalan, R. White, Int. J. Energy Res. 34 (2010) 152–163.
[26] Y. He, X. Liu, C. Zhang, Z. Chen, Appl. Energy 101 (2013) 808–814.
[27] L. Xu, J. Wang, Q. Chen, Energy Convers. Manag. 53 (2012) 33–39.
[28] H. Zhang, M.-Y. Chow, in: IECON 2010 – 36th Annual Conference on IEEE Industrial Electronics Society, 2010, pp. 1844–1849.
[29] S. Abu-Sharkh, D. Doerffel, J. Power Sources 130 (2004) 266–274.
[30] S. Piller, M. Perrin, A. Jossen, J. Power Sources (2001) 113–120.
[31] H. Dai, Z. Sun, X. Wei, in: ICVES, IEEE International Conference on Vehicular Electronics and Safety, 2006, pp. 342–347.
[32] T. Hu, B. Zanchi, J. Zhao, IEEE Trans. Energy Convers. 26 (3) (2011) 787–798.
[33] F. Sun, R. Xiong, H. He, W. Li, J.E.E. Aussems, Appl. Energy (96) (2012) 378–386.
[34] J. Kim, B.H. Cho, IEEE Trans. Veh. Technol. 60 (9) (2011) 4249–4260.
[35] A. Vasebi, M. Partovibakhsh, S.M. Taghi Bathaee, J. Power Sources (174) (2007) 30–40.
[36] G.L. Plett, J. Power Sources 134 (2004) 262–276.
[37] X. Liu, Y. He, Z. Chen, in: 2nd International Conference on Software Engineering and Data Mining (SEDM), 2010, pp. 27–31.
[38] J. Copetti, F. Chenlo, J. Power Sources 47 (1994) 109–118.
[39] J. Copetti, E. Lorenzo, F. Chenlo, Prog. Photovoltaics 1 (1993) 283–292.
[40] R. Babuska, Fuzzy Modeling for Control, KAP, United States, 1998.
[41] K.J. Astrom, B. Wittenmark, Computer-controlled Systems: Theory and Design, Prentice Hall, 1996.
[42] D. Newlin, R. Ramalakshmi, S. Rajasekaran, in: IEEE International Conference on Green High Performance Computing (ICGHPC), 2013, pp. 1–6.
[43] K. Man, K. Tang, S. Kwong, Genetic Algorithms, Springer-Verlag, 1999.